

Monolithically integrated, resonant-cavity-enhanced dual-band mid-infrared photodetector on silicon

Jianfei Wang, Timothy Zens, Juejun Hu, Piotr Becla, Lionel C. Kimerling et al.

Citation: *Appl. Phys. Lett.* **100**, 211106 (2012); doi: 10.1063/1.4722917

View online: <http://dx.doi.org/10.1063/1.4722917>

View Table of Contents: <http://apl.aip.org/resource/1/APPLAB/v100/i21>

Published by the [American Institute of Physics](#).

Related Articles

Reduction of persistent photoconductivity in ZnO thin film transistor-based UV photodetector

Appl. Phys. Lett. **101**, 031118 (2012)

Subpicosecond electron-hole recombination time and terahertz-bandwidth photoresponse in freestanding GaAs epitaxial mesoscopic structures

Appl. Phys. Lett. **101**, 031111 (2012)

Terahertz wavefront measurement with a Hartmann sensor

Appl. Phys. Lett. **101**, 031103 (2012)

Robust and economical multi-sample, multi-wavelength UV/vis absorption and fluorescence detector for biological and chemical contamination

AIP Advances **2**, 032110 (2012)

Top illuminated inverted organic ultraviolet photosensors with single layer graphene electrodes

Appl. Phys. Lett. **101**, 033302 (2012)

Additional information on *Appl. Phys. Lett.*

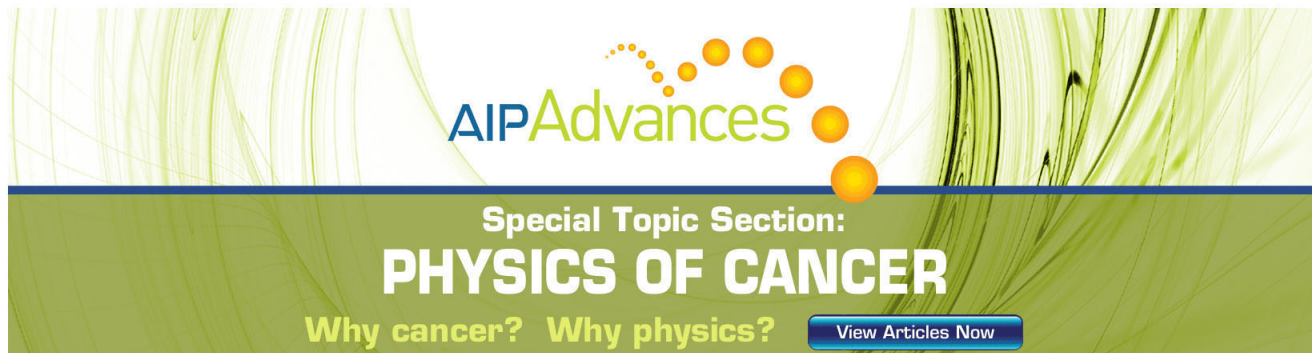
Journal Homepage: <http://apl.aip.org/>

Journal Information: http://apl.aip.org/about/about_the_journal

Top downloads: http://apl.aip.org/features/most_downloaded

Information for Authors: <http://apl.aip.org/authors>

ADVERTISEMENT



AIP Advances

Special Topic Section:
PHYSICS OF CANCER

Why cancer? Why physics? [View Articles Now](#)

Monolithically integrated, resonant-cavity-enhanced dual-band mid-infrared photodetector on silicon

Jianfei Wang,^{1,a)} Timothy Zens,¹ Juejun Hu,² Piotr Becla,¹ Lionel C. Kimerling,¹ and Anuradha M. Agarwal¹

¹*Microphotonics Center, Massachusetts Institute of Technology, 77 Massachusetts Avenue, Cambridge, Massachusetts 02139, USA*

²*Department of Materials Science and Engineering, University of Delaware, Newark, Delaware 19716, USA*

(Received 9 April 2012; accepted 11 May 2012; published online 24 May 2012)

In this paper, we present experimental demonstration of a resonant-cavity-enhanced mid-infrared photodetector monolithically fabricated on a silicon substrate. Dual-band detection at 1.6 μm and 3.7 μm is achieved within a single detector pixel without cryogenic cooling, by using thermally evaporated nanocrystalline PbTe as the photoconductive absorbers. Excellent agreement between theory and experiment is confirmed. The pixel design can potentially be further extended to realizing multispectral detection. © 2012 American Institute of Physics. [<http://dx.doi.org/10.1063/1.4722917>]

Multispectral infrared (IR) detection has been widely employed in hyperspectral imaging, IR spectroscopy, and target identification. Traditional multispectral technology is based on the combination of single spectral focal plane arrays (FPAs) and spectral filters or spectrometers, which requires bulky high-cost mechanical scanning instruments and has a slow response. Single pixels capable of detecting multiple wavebands simultaneously thus have become the focus of third generation FPA development.¹ Recently, multispectral IR detection has been demonstrated in HgCdTe photodiodes,^{2,3} multicolor quantum-well IR photodetectors (QWIPs),¹ and InAs/GaSb type-II superlattice.^{4,5} However, these devices require complicated fabrication and growth of exotic single-crystalline alloys using expensive molecular beam epitaxy (MBE) or metalorganic chemical vapor deposition (MOCVD). Additionally, integration of the FPAs and silicon readout integrated circuits (Si ROIC) relies on hybrid flip-chip bonding, which limits the yield and results in high device cost.^{1,6} Multispectral detection using monolithically integrated pixels will enable dramatically simplified system design with superior mechanical robustness, and thus has attracted a lot of interest around the world today.

Lead chalcogenides (PbS, PbSe, and PbTe) are promising material candidates for mid-IR detection (2–5 μm wavelength) because of their superior chemical and mechanical stability. Integration of single spectral lead chalcogenide photodetectors and Si ROIC has been demonstrated for epitaxial PbTe photodiodes⁷ and polycrystalline PbSe photoconductors.⁸ Nanocrystalline PbTe films have been studied extensively for mid-IR detection sensitized at room temperature by the diffused oxygen, enabling monolithic integration with Si ROIC.^{9–12}

In our previous work, we propose and theoretically analyze the concept of phase-tuned propagation of resonant modes in cascaded planar resonant cavities for multispectral infrared detection.¹³ The building blocks of the multispectral photodetector, i.e., single waveband resonant-cavity-enhanced (RCE) photodetector has been designed and fabri-

cated on a Si platform for mid-IR single-band detection at 3.5 μm wavelength.¹⁴ In this paper, we experimentally demonstrate dual waveband RCE photodetectors on a Si platform with two detection bands located at near-IR (1.6 μm) and mid-IR (3.7 μm), respectively. Room-temperature-sensitized, nanocrystalline PbTe films^{11,12} are used in our device as the IR absorber layers. The device structure is fabricated via multi-step lift-off patterning¹⁵ and the entire fabrication process is accomplished at relatively low temperature (<160 °C), compatible with monolithic integration with Si ROIC.

Fig. 1(a) schematically shows the detector pixel structure fabricated on oxide-coated silicon wafers. The pixel fabrication involves four lift-off steps, which pattern the structure in the following sequence: (1) bottom quarter-wavelength stack (QWS) and mid-IR (3.7 μm band) PbTe absorber; (2) top QWS of the mid-IR cavity, coupling-matching layer, bottom QWS of the near-IR (1.6 μm band) cavity, and the near-IR PbTe absorber; (3) top QWS of the 1.6 μm cavity; and (4) Sn metal contacts. An unpatterned stack with identical layer structures are deposited onto optically polished CaF₂ discs for optical measurement.

Figs. 1(b) and 1(c) show the cross-sectional SEM image of the dual waveband RCE photodetector deposited onto a SiO₂/Si substrate, and for comparison, Fig. 1(d) shows a schematic of the multi-layer design. All 29 layers are clearly identified in the SEM image. Sharp interfaces between the layers indicate negligible material inter-diffusion since the processing temperatures are low (<160 °C).

The dual waveband photodetector uses 50 nm and 100 nm thick PbTe layers as the absorbers for 1.6 μm and 3.7 μm resonant cavity modes, respectively. In comparison, a conventional freespace PbTe photodetector operating at 3.7 μm wavelength requires an absorber layer as thick as 10 μm . A consequence of the thin PbTe detector layer is that the generation-recombination and Johnson noise are reduced by one order of magnitude, since both types of noise scale with the square root of the active material volume. Between the two cavities, a Ge layer of 340 nm was inserted as the coupling-matching layer, which guarantees that the critical coupling condition is met for both cavities and the quantum efficiencies at both IR bands reach maximum.¹³

^{a)}Author to whom correspondence should be addressed. Electronic mail: wangjf05@mit.edu.

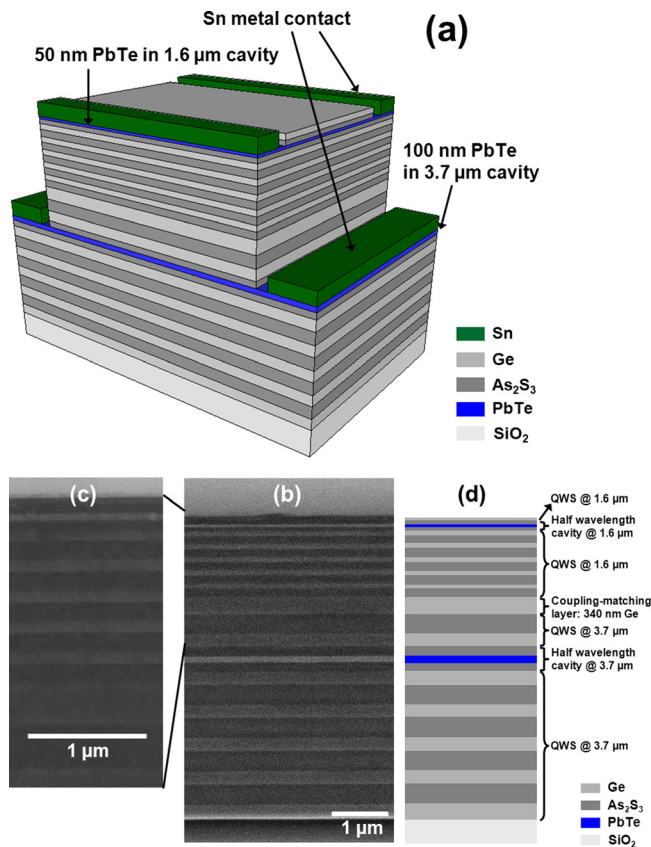


FIG. 1. (a) Three-dimensional schematic picture of the dual waveband RCE photodetector on a Si platform with two resonant cavity modes designed for near-IR ($1.6\ \mu\text{m}$) and mid-IR ($3.7\ \mu\text{m}$). (b) SEM cross-sectional image of the dual waveband RCE photodetector deposited onto a SiO_2/Si substrate. (c) SEM cross-sectional image with higher magnification to show details of the $1.6\ \mu\text{m}$ resonant cavity structure. (d) Schematic picture of the designed structure. All 29 layers are clearly seen in (b) and (c), demonstrating good film thickness control and uniformity. Sharp interfaces between different layers indicate negligible material inter-diffusion occurs since processing temperatures are low ($<160^\circ\text{C}$).

Fig. 2 shows excellent agreement between the simulated (via the transfer matrix method (TMM)) and experimentally measured (using UV-Vis and FTIR spectrometers) reflectance spectra of the dual cavity structure. In the TMM simulation, refractive indices of the QWS materials (As_2S_3 and Ge) are calculated from their transmittance spectra using the

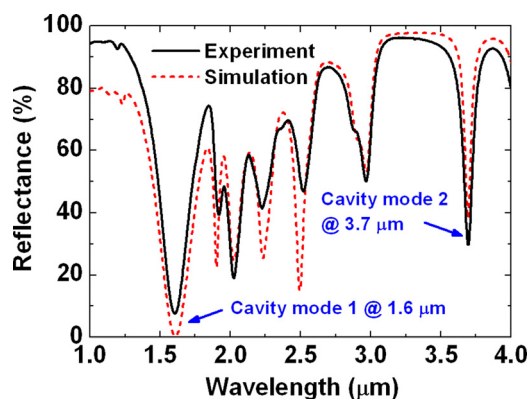


FIG. 2. Reflectance spectra of the dual waveband RCE photodetector obtained by UV-Vis spectroscopy and FTIR measurement (solid line) and TMM simulation (dotted line), showing excellent agreement. The spectra feature two resonant cavity modes which are clearly identified at $1.6\ \mu\text{m}$ and $3.7\ \mu\text{m}$.

TABLE I. Summary of measured fractional peak optical absorption values, FWHM, and quality factors for $1.6\ \mu\text{m}$ and $3.7\ \mu\text{m}$ resonant cavity modes.

	Cavity mode 1	Cavity mode 2
Central wavelength (μm)	1.6	3.7
FWHM (nm)	271	82
Quality factor	6	45
Fractional peak optical absorption (%)	92.3	67.9

Swanepoel approach.¹⁶ The refractive indices of PbTe IR absorber are measured using IR ellipsometry.¹¹ The spectra in Fig. 2 feature two resonant cavity modes at $1.6\ \mu\text{m}$ and $3.7\ \mu\text{m}$ wavelengths. Fractional optical absorption values at the two bands are calculated from measured peak reflectance and transmittance, and are summarized in Table I. Spectral full widths at half maximum (FWHM) are 271 nm and 82 nm for the $1.6\ \mu\text{m}$ and $3.7\ \mu\text{m}$ cavity modes, respectively, corresponding to quality factors of 6 and 45. The relatively low cavity quality factor at the near-IR band is consistent with the large optical absorption coefficient of PbTe at this wavelength.

To quantify photoconductivity of the fabricated detectors, light from a 100 W quartz tungsten halogen (QTH) lamp is modulated and monochromatized using a Newport Oriel MS257 monochromator. Long-pass optical filters are used to block high order diffraction light. A pyroelectric detector with known photo-responsivity is used as a reference detector to obtain the power spectral density of the monochromatic source. A thermoelectric cooler (TEC) is used to cool samples down to -60°C and a Keithley 6220 current source is used to provide bias current. In the photoconductivity measurement, the detectors are biased under fixed current of 0.02 mA, and the photovoltage generated by IR light illumination is recorded. The wavelength resolution in the photoconductivity measurement is $\sim 20\ \text{nm}$ in near-IR and $\sim 45\ \text{nm}$ in mid-IR. Two photoconductive signal peaks are clearly identified in the photoconductivity response shown in Fig. 3, and the peak wavelengths are consistent with the optical measurement in Fig. 2. Peak responsivity values of 28.5 V/W and 13.5 V/W are measured at the resonant wavelengths of $1.6\ \mu\text{m}$ and $3.7\ \mu\text{m}$.

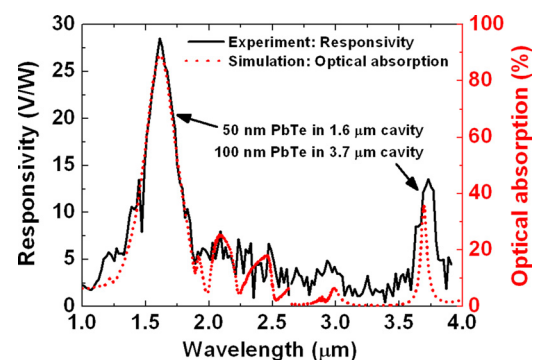


FIG. 3. Responsivity spectra (photoconductivity experiment) and optical absorption spectra (TMM simulation) of the 50 nm and 100 nm PbTe absorbing layers for near-IR and mid-IR detection, demonstrating the operation of the nanocrystalline PbTe based dual waveband RCE photodetector. The discontinuity at $2.6\ \mu\text{m}$ is due to independent experiment/simulation for 50 nm (for near-IR) and 100 nm (for mid-IR) PbTe absorbers, respectively.

Fig. 3 also overlays the TMM simulated optical absorption spectra of the 50 nm (near-IR absorber) and 100 nm (mid-IR absorber) PbTe layers. In general, the absorption spectra match well with the responsivity spectra. Peak optical absorption values of 89% and 36% are demonstrated and their ratio (2.47) is consistent with peak photoconductive signal ratio (2.11). Such high absorption and peak responsivity support the design methodology proposed in our previous study. Analysis of noise mechanisms including background, generation-recombination, and Johnson noises in the photoconductor identifies Johnson noise as the dominant noise.^{6,14} Johnson-noise-limited detectivity of up to $0.72 \times 10^9 \text{ cmHz}^{1/2} \text{ W}^{-1}$ has been obtained in a 100 μm wide RCE photodetector while photoactive layer's thickness is only 100 nm, comparable with commercial polycrystalline mid-IR photodetectors fabricated via chemical bath deposition.¹⁴ Further optimization of the photodetector structure will lead to higher detectivity value ($\sim 10^{10} \text{ cmHz}^{1/2} \text{ W}^{-1}$).

To summarize, we experimentally demonstrate single photodetector pixels capable of detecting near-IR (1.6 μm) and mid-IR (3.7 μm) wavebands simultaneously. Our theoretical simulations and optical/electrical measurement results show excellent agreement. While here we show the proof-of-concept demonstration of dual-band detection, the detector design can be further extended to detect three or more wave bands.¹³ Our approach combines multispectral detection capability, resonant cavity signal enhancement, as well as the potential for Si ROIC monolithic integration, and thus anticipates application venues in imaging and spectroscopic sensing.

This work is supported by the Singapore DSO National Laboratories. The authors would like to thank Microsystems Technology Laboratories (MTL) at MIT for fabrication

facilities and the Center for Materials Science and Engineering (CMSE) at MIT for characterization facilities. The authors also acknowledge Dr. Xiaochen Sun for providing the TMM simulation codes.

- ¹A. Rogalski, J. Antoszewski, and L. Faraone, *J. Appl. Phys.* **105**(9), 091101 (2009).
- ²L. G. Hipwood, C. L. Jones, C. D. Maxey, H. W. Lau, J. Fitzmaurice, R. A. Catchpole, and M. Ordish, *Proc. SPIE* **6206**, 620612 (2006).
- ³D. F. King, W. A. Radford, E. A. Patten, R. W. Graham, T. F. McEwan, J. G. Vodicka, R. E. Bornfreund, P. M. Goetz, G. M. Venzor, and S. M. Johnson, *Proc. SPIE* **6206**, 62060W (2006).
- ⁴R. Rehm, M. Walther, J. Schmitz, J. Fleißner, J. Ziegler, W. Cabanski, and R. Breiter, *Proc. SPIE* **6294**, 629404 (2006).
- ⁵E. K. Huang, A. Haddadi, G. Chen, B. Nguyen, M. Hoang, R. McClintock, M. Stegall, and M. Razeghi, *Opt. Lett.* **36**(13), 2560–2562 (2011).
- ⁶J. Wang, Ph.D. dissertation, Massachusetts Institute of Technology, Cambridge, 2010.
- ⁷J. John and H. Zogg, *J. Appl. Phys.* **85**(6), 3364–3367 (1999).
- ⁸G. Vergara, M. Montojo, M. Torquemada, M. Rodrigo, F. Sanchez, L. Gomez, R. Almazan, M. Verdu, P. Rodriguez, V. Villamayor, M. Alvarez, J. Diezhandino, J. Plaza, and I. Catalan, *Opto-Electron. Rev.* **15**, 110–117 (2007).
- ⁹Z. Dashevsky, R. Kreizman, and M. P. Dariel, *J. Appl. Phys.* **98**, 094309 (2005).
- ¹⁰T. Komissarova, D. Khokhlov, L. Ryabova, Z. Dashevsky, and V. Kasiyan, *Phys. Rev. B* **75**, 195326 (2007).
- ¹¹J. Wang, J. Hu, X. Sun, A. M. Agarwal, L. C. Kimerling, D. R. Lim, and R. A. Synowicki, *J. Appl. Phys.* **104**, 053707 (2008).
- ¹²J. Wang, J. Hu, P. Becla, A. Agarwal, and L. C. Kimerling, *J. Appl. Phys.* **110**, 083719 (2011).
- ¹³J. Wang, J. Hu, X. Sun, A. Agarwal, and L. C. Kimerling, *Opt. Lett.* **35**(5), 742–744 (2010).
- ¹⁴J. Wang, J. Hu, P. Becla, A. Agarwal, and L. C. Kimerling, *Opt. Express* **18**(12), 12890–12896 (2010).
- ¹⁵J. Hu, V. Tarasov, N. Carlie, L. Petit, A. Agarwal, K. Richardson, and L. C. Kimerling, *Opt. Mater.* **30**(10), 1560–1566 (2008).
- ¹⁶R. Swanepoel, *J. Phys. E* **16**(12), 1214–1222 (1983).